High trapping forces for high-refractive index particles trapped in dynamic arrays of counterpropagating optical tweezers

Astrid van der Horst,[1,2,3,*] Peter D. J. van Oostrum,[2] Alexander Moroz,[2,4] Alfons van Blaaderen,[2] and Marileen Dogterom[1]

[1]Fundamenteel Onderzoek der Materie (FOM) Institute for Atomic and Molecular Physics (AMOLF), Kruislaan 407, 1098 SJ Amsterdam, The Netherlands

[2]Soft Condensed Matter, Debye Institute for Nanomaterials Science, Utrecht University, Princetonplein 5, 3584 CC Utrecht, The Netherlands

[3]Currently at Department of Physics, Simon Fraser University, 8888 University Drive, Burnaby, British Columbia V5A 1S6, Canada

[4]Currently at www.wave-scattering.com

*Corresponding author: astrid.van.der.horst@sfu.ca

We demonstrate the simultaneous trapping of multiple high-refractive index ($n > 2$) particles in a dynamic array of counterpropagating optical tweezers in which the destabilizing scattering forces are canceled. These particles cannot be trapped in single-beam optical tweezers. The combined use of two opposing high-numerical aperture objectives and micrometer-sized high-index titania particles yields an at least threefold increase in both axial and radial trap stiffness compared to silica particles under the same conditions. The stiffness in the radial direction is obtained from measured power spectra; calculations are given for both the radial and the axial force components, taking spherical aberrations into account. A pair of acousto-optic deflectors allows for fast, computer-controlled manipulation of the individual trapping positions in a plane, while the method used to create the patterns ensures the possibility of arbitrarily chosen configurations. The manipulation of high-index particles finds its application in, e.g., creating defects in colloidal photonic crystals and in exerting high forces with low laser power in, for example, biophysical experiments.   © 2008 Optical Society of America

OCIS codes: 140.7010, 170.4520, 230.1040.

1. Introduction

In 1986, Ashkin *et al.* introduced the optical trapping of dielectric particles using a single-beam gradient trap [1]. In such a configuration, known as optical tweezers, a large gradient in light intensity is created by tightly focusing a laser beam using a high-numerical aperture (NA) objective. For particles with a refractive index n_p higher than the index n_m of the surrounding medium, this gradient provides the necessary force F_{grad} to balance the destabilizing scattering force F_{sc}. In general, an increase in n_p or in the radius r of the particle yields an increase in these forces, but the dependence on r and on $m = n_p/n_m$ is stronger for F_{sc} than for F_{grad}. This can clearly be seen in the Rayleigh regime ($r \ll \lambda$, the wavelength of the trapping laser), where these dependencies are given by $F_{sc} \sim r^6(m^2 - 1)^2/(m^2 + 2)^2$ and $F_{grad} \sim r^3(m^2 - 1)/(m^2 + 2)$ [1]. For our particles, with $r \simeq \lambda$ in the Mie regime, interactions are not described correctly by Rayleigh scattering and the force relations are

more complicated. Also, although the physically insightful decomposition of the interaction of light with particles of this size into F_{sc} and F_{grad} becomes less meaningful, formally it can still be done, and one finds that also for these particles F_{sc} depends more strongly on r and m than does F_{grad}. This limits the size and refractive index of particles that can be trapped in a single-beam gradient trap and, with this, a limit is set to the trapping force of a single-beam gradient trap.

By using a second, counterpropagating trapping beam, the radiation pressure in the propagation direction can be canceled. Such counterpropagating or dual-beam traps have been used before in several configurations [2–6]. In these cases, however, the focusing of the laser beam was mild, either due to the use of low-NA objectives or because the diameter of the beam was kept small in comparison with the aperture of the objectives; the possibility of a high trapping force for a counterpropagating trap was, therefore, not fully exploited.

Here we demonstrate the trapping of high-refractive index titania particles in an array of counterpropagating traps of which the positions can be dynamically changed. We combine this counterpropagating trapping with overfilling of the two high-NA objectives, thereby canceling the radiation pressure, while a large intensity gradient provides a high trap stiffness. The array of counterpropagating traps was created by time-sharing the laser beam over the positions of the array using a pair of acousto-optic deflectors (AODs), ensuring fast, computer-controlled dynamics of the individual traps in a plane. The possibility of trapping an array of high-index particles at once, and being able to manipulate individual particles within such an array independently, finds its application in, for example, manipulating high-refractive index rodlike particles in three dimensions (3D), e.g., ZnO nanorods [7]; patterning surfaces for colloidal epitaxy [8]; and creating defects in colloidal photonic crystals. For titania and silica particles, the radial stiffness was derived from measured power spectral density (PSD) curves [9]. In addition, calculations were done to obtain both the axial stiffness and the radial stiffness [10,11], including taking spherical aberrations due to the use of an oil immersion objective to trap in ethanol into account [12]. Both the measurements and the calculations show higher trap stiffnesses for titania particles compared to silica particles under the same conditions. Also, the effects of the use of high-NA objectives, particle radius r, and refractive index n on the trap stiffness are investigated using calculations.

2. Experimental Methods

To allow for counterpropagating trapping in our setup [Fig. 1(a)], the condenser of an inverted microscope (Leica DM IRB) is replaced by a high-NA objective [7,13]. The distance between the two objectives (both: Leica 100×, 1.4 NA, oil immersion) is 0.52 mm when overlapping their focal planes. An in-
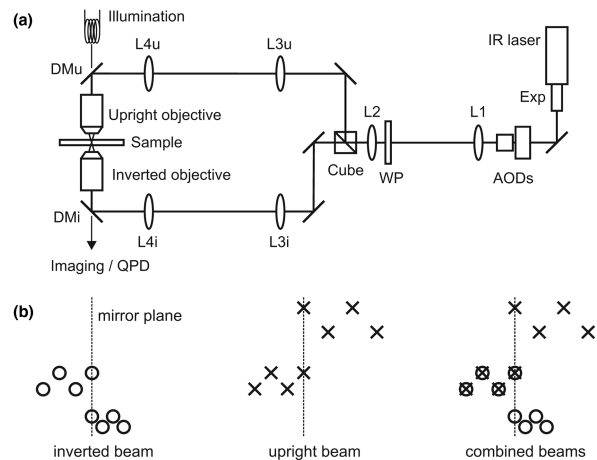

Fig. 1. Schematics of (a) the optical tweezers setup and (b) the counterpropagating traps scanned with one pair of AODs. A pattern of inverted beam traps (∘) is a mirror image of the pattern of upright beam traps (×) with the mirror plane top-to-bottom in the image. In addition, the magnification between the inverted and the upright beam path might differ. By adding a mirrored and appropriately scaled pattern to the original traps, counterpropagating traps (⊗) can be created for which the position of each trap can be chosen arbitrarily.

frared laser beam (Spectra Physics Millennia, 1064 nm, 10 W cw) is split at a polarizing beam splitter cube, while the rotation of the wave plate (WP) determines the ratio between the power sent to the inverted objective and that sent to the upright objective. In both beam paths a pair of lenses (L3$_{i,u}$ and L4$_{i,u}$, all $f = 80$ mm) forms a telescope to provide manual displacement of the laser focus. The use of dichroic mirrors DM$_{i,u}$ allows for illumination and imaging in the visible, including confocal microscopy. Before splitting, the laser beam passes a pair of AODs (IntraAction DTD-276HB6), positioned at a plane conjugate to the back focal planes of the objectives. The signal to the AODs is supplied by direct digital synthesizers (Novatech DDS 8 m) controlled by a LabVIEW (National Instruments) program. By fast repositioning of the laser focus, multiple time-shared traps are created [14]. The position of the traps can be preprogrammed or changed interactively. The beam is expanded in two steps: before the AODs by a 6× beam expander and after the AODs ∼2× by the lenses L1 ($f = 120$ mm) and L2 ($f = 250$ mm). For position detection of a particle in a nonshared trap, the fraction of the infrared beam that leaks through dichroic mirror DM$_i$ is imaged onto a quadrant photodiode (QPD) that is placed at the front camera port of the microscope.

The sample cell, consisting of two coverslips (Menzel No. 1) sealed together with candle wax, was filled with a dilute mixture of SiO$_2$ ($n = 1.45$, diameter 1.4 μm) and TiO$_2$ ($n = 2.4$, diameter 1.1 μm) particles. Ethanol ($n = 1.36$) was the initial dispersion and, because the refractive index of ethanol is close to, though slightly higher than that of water ($n = 1.33$, commonly used in biophysical experiments), we kept the particles dispersed in ethanol.

A pattern scanned by the AODs is imaged inside the sample by both objectives. The upright objective, however, will give a mirror image of the pattern imaged by the inverted objective [see Fig. 1(b)]. To not be limited to symmetric patterns using a single pair of AODs, we scan both the desired pattern and its mirror image. Then, inside the sample, we place the pattern from the inverted beam opposite the mirror image from the upright beam, creating an array of counterpropagating traps. By scaling the added mirror image, we can also compensate for differences in magnification between the inverted and the upright beam paths introduced by the telescopes or by the use of objectives with different magnifications. We aligned the counterpropagating traps by visually checking on the camera image that a trapped silica particle did not change position when the inverted beam and the upright beam were alternately blocked.

3. Experimental Results

The method of creating the counterpropagating trap patterns by also scanning the mirror image allows for rapid manipulation of multiple high-index particles, as can be seen in Fig. 2. Here, stills from a movie show how patterns of eight traps were combined to form four counterpropagating traps (plus eight single-beam traps that were not used). The array of counterpropagating traps, positioned at a distance of $12\,\mu m$ from either wall, was filled with one silica and three titania particles. The total power inside the sample was $44\,mW$, corresponding to $5.5\,mW$ for each individual counterpropagating trap. The pattern was scanned at $4.5\,kHz$ and changed in 34 steps over a total period of $1.2\,s$, yielding an average speed of the particles of $\sim20\,\mu m/s$. In bright-field microscopy, the apparent size of the imaged particles is larger than the actual size [15]. For particles with a higher refractive index this effect is more pronounced, causing the $1.1\,\mu m$ diameter TiO_2 particles

to appear larger than the $1.4\,\mu m$ diameter SiO_2 particle.

Three-dimensional trapping of the TiO_2 particles in single-beam traps was not possible for any of the dozens of particles we tried to trap; they were pushed along the beam axis. This is in accordance with the absence of a stable trapping position for these particles in the single-beam calculations (Presented in Section 4).

We measured the radial trap stiffness κ_x using QPD measurements. By fitting a Lorentzian to the normalized PSD curve of the QPD signal (Fig. 3) we obtained the roll-off frequency f_0 and used $\kappa_x = 12\pi^2\eta r f_0$, with η as the viscosity of the medium [16]. The high-frequency parts of the spectra for titania deviate from the −2 slope typical for Brownian motion. This is possibly caused by not capturing all the light with the high-NA objective for these strongly scattering titania particles. However, we do not expect this to influence f_0 significantly. For these measurements, one stationary counterpropagating trap was used, with powers inside the trap of 22, 44, 88, and, only for the titania particle, $176\,mW$ (measured using the two-objective method [17]). For a power of $44\,mW$ in the sample we found f_0 to be $499\,Hz$ for the $1.1\,\mu m$ diameter TiO_2 particle and, with $\eta = 1.2 \times 10^{-3}\,Ns/m^2$ for ethanol, this yields a stiffness of $\kappa_x = 39\,pN/\mu m$. The trap stiffness increased linearly with increasing laser power. Because of the mechanical noise in the curves for the $1.4\,\mu m$ diameter SiO_2 particle, we fitted these Lorentzians manually. Assuming for the three curves an increase in stiffness linear with laser power, we found at $44\,mW$ an f_0 of $115 \pm 10\,Hz$, corresponding to $\kappa_x = 11.4\,pN/\mu m$, thus, a factor of 3.4 lower stiffness than for the smaller titania particle.

4. Calculations

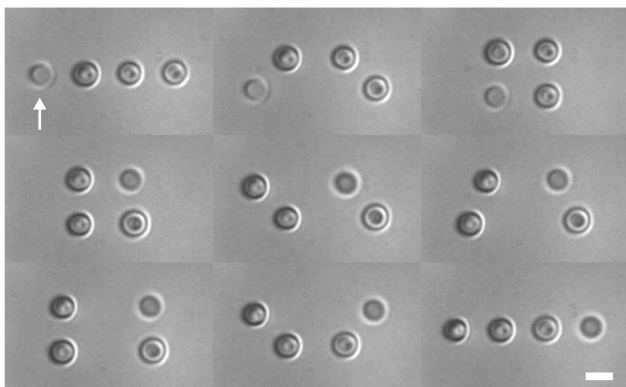For our calculations we used the Mie–Debye representation first given by Maia Neto and Nussenzveig
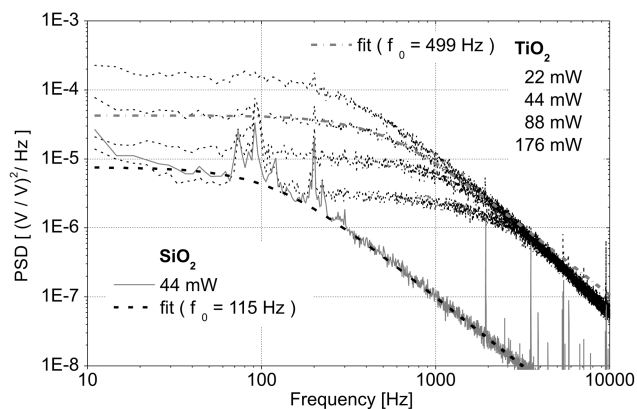
Fig. 2. (Multimedia online; ao.osa.org) Stills from a movie in bright-field microscopy of four counterpropagating traps filled with one $1.4\,\mu m$ diameter SiO_2 (arrow) and three $1.1\,\mu m$ diameter TiO_2 particles. The particles are positioned $12\,\mu m$ away from either wall, and the pattern is changed in 34 steps in $1.2\,s$. The short version of the movie (1.8 MB) shows this complete change of the pattern four times, while the longer version of the movie (12.3 MB) shows it 28 times. Scale bar is $2\,\mu m$.

Fig. 3. PSD curves of the normalized signal for a SiO_2 (gray solid curve, diameter $1.4\,\mu m$) and a TiO_2 (black dotted curves, $1.1\,\mu m$) particle in ethanol for given laser powers inside the counterpropagating trap. For clarity only one curve is shown for SiO_2. Lorentzian fits (dashed curves) are plotted for the $44\,mW$ curves, with f_0 at $115\,Hz$ (SiO_2) and $499\,Hz$ (TiO_2). Highest laser powers result in lowest plateau values.

for the axial direction [10], expanded to 3D by Mazolli and co-workers [11], and complemented by Viana *et al.*[12] to include spherical aberrations (i.e., the focal depth of a light ray depends on the distance of this ray to the optical axis). In these calculations, the parameters describing the laser trap configuration are the beam opening angle θ and γ, the ratio of the objective focal length to the beam waist ω_0. We used $\theta = 64.245°$, $\gamma = 1.21$, and laser wavelength $\lambda = 1064$ nm. The spherical aberrations, due to the refractive index mismatch between the coverslip and the ethanol, depend on the distance from the geometric focus to the glass surface. In our calculations this distance was $12\,\mu\text{m}$.

In Fig. 4(a), the trapping force F per laser power P (at the back focal plane) is plotted ($F/P = Qn_{\text{m}}/c$, with Q the trapping efficiency and c the speed of light). Stable trapping occurs at the position where $F_z = 0$ and $dF_z/dz < 0$. In a single-beam gradient trap a $1.1\,\mu\text{m}$ diameter SiO$_2$ particle (solid curve) will be trapped at a position in front of the focal plane of the objective (negative z) due to the spherical

aberrations [18,19]. For a TiO$_2$ particle of the same size, however, no stable trapping occurs (dashed–dotted curve).

To calculate the force on a particle in a counterpropagating (cp) trap, we averaged the curves for the upright and the inverted beam, which in our experiment have perpendicular polarization. (The curve for the upright trapping beam is the negative of the inverted one, with the z axis mirrored at the position of stable trapping for the $1.4\,\mu\text{m}$ diameter SiO$_2$ particle, corresponding to the experimental configuration.) For the $1.1\,\mu\text{m}$ diameter SiO$_2$ particle we find that the curve for counterpropagating trapping (dashed curve) does not differ much from the curve for single-beam gradient trapping, which is in accordance with the small role played by the scattering force due to the small difference in refractive index between silica and ethanol. For the TiO$_2$ particle in the counterpropagating trap, however, we now find a stable trapping position (dashed curve). We find the axial trap stiffness κ_z (the absolute value of dF_z/dz at the trapping position) to be 877 and $217\,\text{pN}/(\mu\text{m} \times \text{W})$ for $1.1\,\mu\text{m}$ diameter TiO$_2$ and SiO$_2$ in ethanol, respectively. Thus, κ_z is 4× higher for the TiO$_2$ particles than for the SiO$_2$ particle under the same conditions. For $1.4\,\mu\text{m}$ diameter silica particles as used in our experiments $\kappa_z = 192\,\text{pN}/(\mu\text{m} \times \text{W})$, yielding a factor of 4.6 (data not shown).

Figure 4(b) shows the radial forces at $z = -0.628\,\mu\text{m}$ (the calculated position of stable trapping for $1.4\,\mu\text{m}$ SiO$_2$ with $z = 0$ as the geometric focus of the objective). Because of the symmetric configuration, these radial forces are the same for both the single-beam and the counterpropagating configuration. We find stiffnesses of 3754, 1284, and $655\,\text{pN}/(\mu\text{m} \times \text{W})$ for the $1.1\,\mu\text{m}$ TiO$_2$, $1.1\,\mu\text{m}$ SiO$_2$, and $1.4\,\mu\text{m}$ SiO$_2$, respectively, giving for the titania particle an increase in κ_{xy} of 2.9× (compared to $1.1\mu\text{m}$ SiO$_2$) and 5.7× (compared to $1.4\,\mu\text{m}$ SiO$_2$). Also, in the axial as well as the radial direction, we see a higher maximum force for the trapped titania particle as compared to silica.

Spherical aberrations, which spread out the focus of the laser beam and increase the opening angle of the outer light rays, affect the trapping forces [19] and can, depending on the trapping configuration, either increase or decrease trap stiffnesses. We therefore also calculated the axial and radial forces while disregarding these aberrations [10,11]. The absence of spherical aberrations would, for example, be obtained by using water immersion objectives to trap in water. In our calculations, however, we used ethanol to investigate the effects only of the spherical aberrations and not have an added effect of a change in ratio of the refractive indices m. The axial trap stiffness κ_z [Fig. 5(a)] is 1043, 409, and $272\,\text{pN}/(\mu\text{m} \times \text{W})$ for $1.1\,\mu\text{m}$ diameter TiO$_2$ and $1.1\,\mu\text{m}$ and $1.4\,\mu\text{m}$ SiO$_2$ in ethanol, respectively. This corresponds to a κ_z that is 2.6× higher for the TiO$_2$ particle than for the SiO$_2$ particle under the same conditions, while compared to the $1.4\,\mu\text{m}$ diameter silica particles (data not shown) the increase
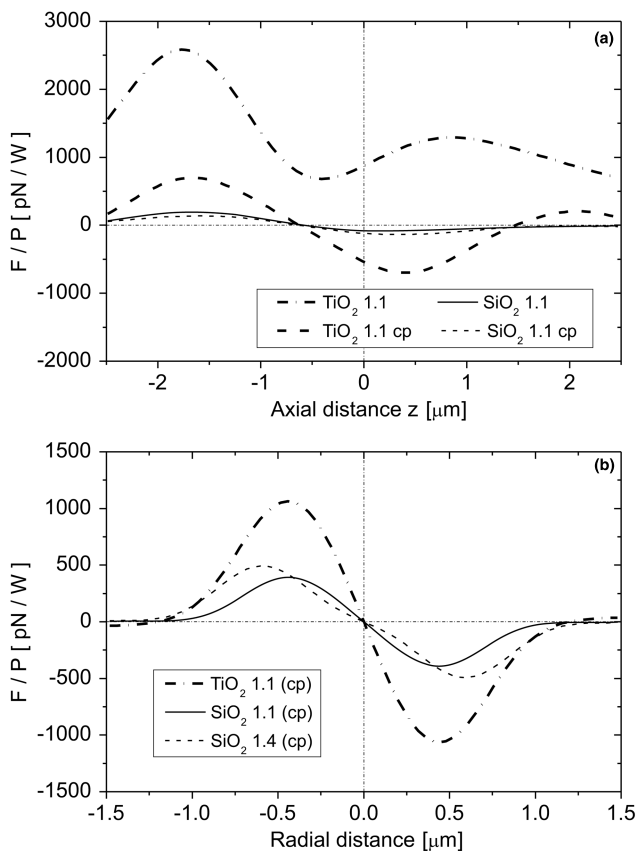
Fig. 4. Calculations of the force per 1 W laser power for $1.1\,\mu\text{m}$ diameter TiO$_2$ ($n = 2.4$) and SiO$_2$ ($n = 1.45$) particles in ethanol ($n = 1.36$) in Gaussian single and cp traps using 100×, 1.4 NA, oil immersion objectives. Spherical aberrations are accounted for. (a) Axial force, with z as the offset of the particle from the focal plane of one objective and (b) radial force at the trapping plane for $1.4\,\mu\text{m}$ SiO$_2$ ($z = -0.628\,\mu\text{m}$) as a function of the distance to the optical axis. In addition, the curve for $1.4\,\mu\text{m}$ SiO$_2$ is shown.
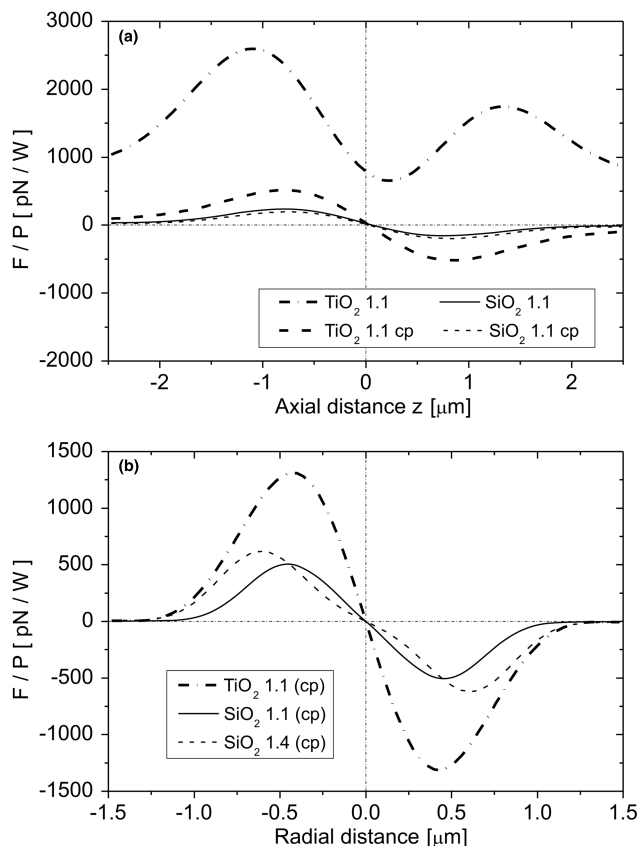
Fig. 5. Calculations of the force per 1 W laser power for $1.1\,\mu m$ diameter TiO_2 ($n = 2.4$) and SiO_2 ($n = 1.45$) particles in ethanol ($n = 1.36$) in Gaussian single and cp traps using 100×, 1.4 NA, oil immersion objectives. Spherical aberrations are neglected. (a) Axial force, with z as the offset of the particle from the focal plane of one objective and (b) radial force at the trapping plane for $1.4\,\mu m$ SiO_2 ($z = 0.028\,\mu m$) as a function of the distance to the optical axis. In addition, the curve for $1.4\,\mu m$ SiO_2 is shown.

is 3.8×. The code to calculate these axial forces without spherical aberrations, based on [10], is made available online [20]. For the radial stiffness κ_{xy} [Fig. 5 (b)] we find 4921, 1399, and 732 pN/$(\mu m \times W)$ for the $1.1\,\mu m$ diameter TiO_2, $1.1\,\mu m$ SiO_2 (increase is 3.5×), and $1.4\,\mu m$ SiO_2 (6.7×), respectively. Also here the maximum forces are higher for titania than for silica. The shown radial results are for $z = 0.028\,\mu m$, the calculated position of stable trapping for $1.4\,\mu m$ SiO_2 in ethanol, chosen as the plane of symmetry for the counterpropagating beams when spherical aberrations are not included.

The trapping forces are not only influenced by the refractive indices, but also by the distance between the focal planes of the objectives, the beam diameter with respect to their back apertures, and the particle's size parameter $\beta = r/\lambda$. The dependencies are nonlinear and these parameters have not been optimized in our experiments nor in our calculations. To illustrate this, we calculated for a varying refractive index n, trap stiffnesses κ_z and κ_{xy} for a $1.4\,\mu m$ diameter particle in ethanol. The curves in Fig. 6, with and without

spherical aberrations taken into account, show that our experimentally used titania ($n = 2.4$) does not give the largest increase in trap stiffness, neither axial nor radial. In addition, we investigated the oscillations in Q, due to Mie resonances, for increasing size parameter β, seen both experimentally [21,22] as well as in calculations [10,22]. We plotted κ_z and κ_{xy} as functions of the particle radius r for titania [Fig. 7 (a)] and silica [Fig. 7(b)] in ethanol. The calculations took spherical aberrations into account and were done for a single position—on the optical axis at $z = -0.628\,\mu m$ our chosen plane of symmetry for the counterpropagating beam configuration, as dictated by the silica particles used. For the titania particles this position is not for every r the position for which $F_z = 0$ (i. e., the axial trapping position). However, these results do give an indication of the large variations in trap stiffness for changes in particle size, especially for titania.

To investigate our choice for using high-NA (100×, 1.4 NA) objectives, we compare the calculations with those for low-NA (60×, 0.85 NA) objectives as used in several other counterpropagating tweezer configurations [4,5]. Figure 8 shows the results for the counterpropagating trapping of a $1.1\,\mu m$ diameter TiO_2 particle in ethanol. In the radial direction the stiffnesses are 4921 and 3085 pN/$(\mu m \times W)$ for 1.4 NA and 0.85 NA, respectively (data not shown), while the axial stiffnesses are 1043 and 103 pN/$(\mu m \times W)$, respectively. The use of high-NA objectives yields a large increase in trap stiffness, especially in the axial direction. (These results are in accordance with the results of Rodrigo $et\ al.$ [23] for their counterpropagating generalized phase contrast method; their calculated trapping efficiencies using low-NA objectives are an order of magnitude lower than what we find for our high-NA objective configuration.)
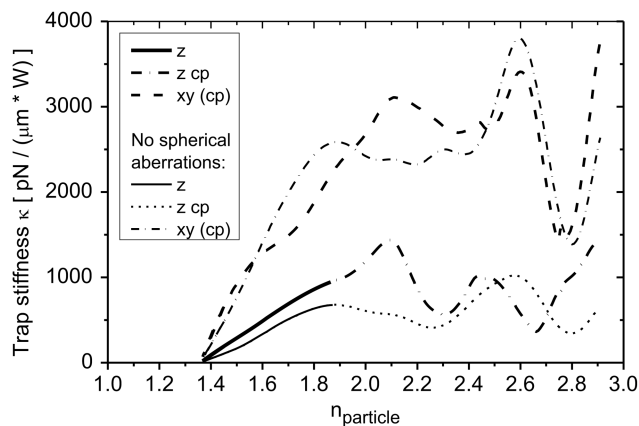

Fig. 6. Calculated trap stiffness κ for varying indices of refraction n of a $1.4\,\mu m$ diameter particle in ethanol ($n = 1.36$) with and without spherical aberrations. Single-beam trapping (solid curves) is limited to $n < 1.87$; for higher n the particle will be pushed along the beam axis. Because of symmetry, where single-beam trapping is possible, the radial stiffness κ_{xy} is the same as κ_{xy} for cp trapping.
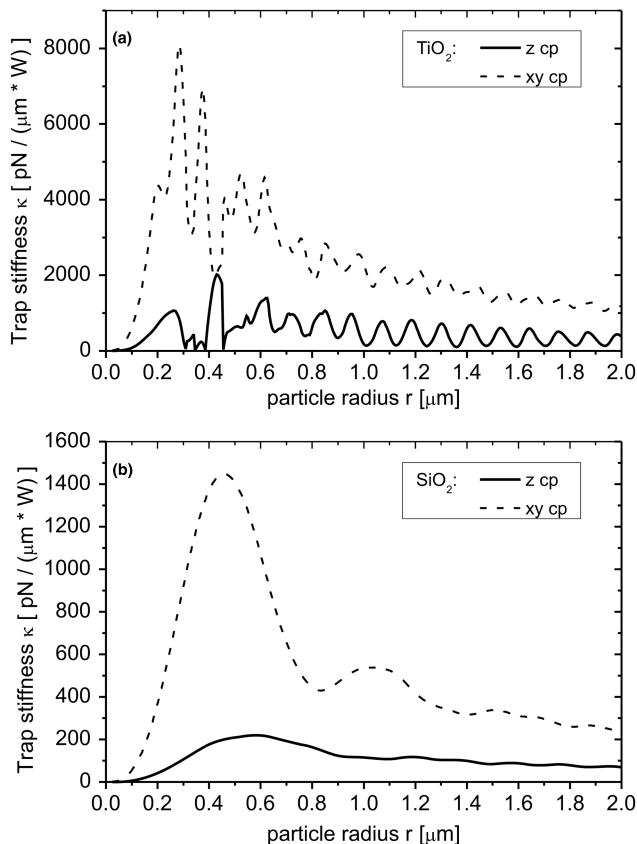
Fig. 7. Calculated trap stiffness κ_z and κ_{xy} for varying radius r of (a) titania ($n = 2.4$) and (b) silica ($n = 1.45$) particles in cp traps in ethanol ($n = 1.36$). The stiffness is calculated at fixed depth $z = -0.628\,\mu$m, which is not for every radius the position for which $F_z = 0$. Spherical aberrations were taken into account.

5. Conclusions and Discussion

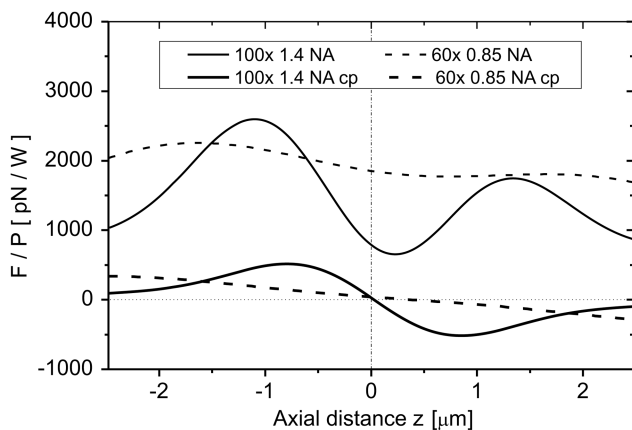We demonstrated the trapping of high-refractive index particles in counterpropagating optical tweezers

Fig. 8. Calculated axial force (assuming no spherical aberrations) for a $1.1\,\mu$m diameter TiO_2 particle ($n = 2.4$) in ethanol ($n = 1.36$) for high-NA objectives (100×, 1.4 NA; solid curves) and low-NA objectives (60×, 0.85 NA; dashed curves). There is no stable trapping position for the single-beam traps. In the counterpropagating (cp) beams, the axial stiffness κ_z at the stable trapping position is $1043\,pN/(\mu m \times W)$ (1.4 NA) and $103\,pN/(\mu m \times W)$ (0.85 NA).

and found that, as expected from our calculations, these particles could not be trapped in single-beam optical tweezers. In our calculations we compared counterpropagating trapping with high-NA objectives, as used in our experiments, with that of low-NA objectives, as used by several others [4,5]. Although it should be noted that the axial position of the beams was not optimized in either of the cases, the use of high-NA objectives yields a large increase in obtainable axial trap stiffness.

From our calculations between the optimal trapping size for a silica particle and a titania particle it follows that for counterpropagating traps $0.86\,\mu$m diameter tiania particles can be trapped 9× stronger axially than optimally sized silica particles ($1.16\,\mu$m in diameter). These calculations do not take polarization of the laser light, beam misalignment, transmittance of the objectives, or radial dependency of the transmittance [24] into account. Also, any interference of the focused high-NA laser beams [25] has not been included. Therefore, our results give an upper bound of the increase in trap stiffness that can be expected for particles with an index of $n = 2.4$ in ethanol.

In addition, the measured threefold increase in radial trap stiffness for a $1.1\,\mu$m diameter TiO_2 particle compared to a $1.4\,\mu$m diameter SiO_2 particle in ethanol indicates that the use of high-index particles combined with counterpropagating optical tweezers is indeed a promising method to exert high forces at low laser powers. Our calculations for this experimental configuration show an even higher obtainable increase (6.7×). These results are relevant also for aqueous solutions (H_2O, $n = 1.33$) used in most biological applications, as the difference in refractive index as compared to ethanol is small. The discrepancy between the absolute values of calculated and measured forces might be due to many factors, including differences in the particle diameters, refractive indices, beam alignment, effects of polarization in the focus, and beam diameter. All these parameters play a role in the increase of trapping forces, with nonlinear dependencies, such as the Mie resonances for increasing particle size. However, calculations can be useful in sampling the expansive parameter space to optimize trap stiffness or, e.g., maximum trapping force.

The method of scanning both the pattern and its mirror image provides flexibility in manipulating multiple high-index particles by supplying the possibility of arbitrarily chosen dynamic configurations of the counterpropagating traps while avoiding the cost of a second pair of AODs.

References

1. A. Ashkin, J. M. Dziedzic, J. E. Bjorkholm, and S. Chu, "Observation of a single-beam gradient force optical trap for dielectric particles," Opt. Lett. **11**, 288–290 (1986).

2. A. Ashkin, "Acceleration and trapping of particles by radiation pressure," Phys. Rev. Lett. **24**, 156–159 (1970).

3. S. B. Smith, Y. Cui, and C. Bustamante, "Overstretching B-DNA: the elastic response of individual double-stranded and single-stranded DNA molecules," Science **271**, 795–799 (1996).

4. P. J. Rodrigo, V. R. Daria, and J. Glückstad, "Real-time three-dimensional optical micromanipulation of multiple particles and living cells," Opt. Lett. **29**, 2270–2272 (2004).

5. W. Wang, A. E. Chiou, G. J. Sonek, and M. W. Berns, "Self-aligned dual-beam optical laser trap using photorefractive phase conjugation," J. Opt. Soc. Am. B **14**, 697–704 (1997).

6. W. Grange, S. Husale, H.-J. Güntherodt, and M. Hegner, "Optical tweezers system measuring the change in light momentum flux," Rev. Sci. Instrum. **73**, 2308–2316 (2002).

7. A. van der Horst, A. I. Campbell, L. K. van Vugt, D. A. M. Vanmaekelbergh, M. Dogterom, and A. van Blaaderen, "Manipulating metal-oxide nanowires using counter-propagating optical line tweezers," Opt. Express **15**, 11629–11639 (2007).

8. J. P. Hoogenboom, D. J. L. Vossen, C. Faivre-Moskalenko, M. Dogterom, and A. van Blaaderen, "Patterning surfaces with colloidal particles using optical tweezers," Appl. Phys. Lett. **80**, 4828–4830 (2002).

9. K. Svoboda and S. Block, "Biological applications of optical forces," Annu. Rev. Biophys. Biomol. Struct. **23**, 247–285 (1994).

10. P. A. Maia Neto and H. M. Nussenzveig, "Theory of optical tweezers," Europhys. Lett. **50**, 702–708 (2000).

11. A. Mazolli, P. A. Maia Neto, and H. M. Nussenzveig, "Theory of trapping forces in optical tweezers," Proc. R. Soc. London Ser. A **459**, 3021–3041 (2003).

12. N. B. Viana, M. S. Rocha, O. N. Mesquita, A. Mozolli, P. A. Maia Neto, and H. M. Nussenzveig. "Towards absolute calibration of optical tweezers," Phys. Rev. E **75**, 021914 (2007).

13. D. L. J. Vossen, A. van der Horst, M. Dogterom, and A. van Blaaderen, "Optical tweezers and confocal microscopy for simultaneous three-dimensional manipulation and imaging in concentrated colloidal dispersions," Rev. Sci. Instrum. **75**, 2960–2970 (2004).

14. K. Visscher, S. P. Gross, and S. M. Block, "Construction of multiple-beam optical traps with nanometer-resolution position sensing," IEEE J. Sel. Top. Quantum Electron. **2**, 1066–1076 (1996).

15. J. Baumgartl and C. Bechinger., "On the limits of digital microscopy," Europhys. Lett. **71**, 487–493 (2005).

16. M. W. Allersma, F. Gittes, M. J. deCastro, R. J. Stewart, and C. F. Schmidt, "Two-dimensional tracking of ncd motility by back focal plane interferometry," Biophys. J. **74**, 1074–1085 (1998).

17. H. Misawa, M. Koshioka, K. Sasaki, N. Kitamura, and H. Masuhara, "Three-dimensional optical trapping and laser ablation of a single polymer latex particle in water," J. Appl. Phys. **70**, 3829–3836 (1991).

18. A. C. Dogariu and R. Rajagopalan, "Optical traps as force transducers: the effects of focusing the trapping beam through a dielectric interface," Langmuir **16**, 2770–2778 (2000).

19. A. Rohrbach and E. H. K. Stelzer, "Trapping forces, force constants, and potential depths for dielectric spheres in the presence of spherical aberrations," Appl. Opt. **41**, 2494–2507 (2002).

20. The code to calculate the axial forces is freely available on www.wave-scattering.com and as supplementary material to this paper.

21. A. Ashkin and J. M. Dziedzic, "Observation of resonances in the radiation pressure on dielectric spheres," Phys. Rev. Lett. **38**, 1351–1355 (1977).

22. A. A. R. Neves, A. Fontes, L. de Y. Pozzo, A. A. de Thomaz, E. Chillce, E. Rodriguez, L. C. Barbosa, and C. L. Cesar, "Electromagnetic forces for an arbitrary optical trapping of a spherical dielectric," Opt. Express **14**, 13101–13106 (2006).

23. P. J. Rodrigo, I. R. Perch-Nielsen, and J. Glückstad, "Three-dimensional forces in GPC-based counterpropagating-beam traps," Opt. Express **14**, 5812–5822 (2006).

24. N. B. Viana, M. S. Rocha, O. N. Mesquita, A. Mozolli, and P. A. Maia Neto, "Characterization of objective transmittance for optical tweezers," Appl. Opt. **45**, 4263–4269 (2006).

25. B. Richards and E. Wolf, "Electromagnetic diffraction in optical systems. II. Structure of the image field in an aplanatic system," Proc. R. Soc. London Ser. A **253**, 358–379 (1959).